Geosci. Model Dev. Discuss., 5, 2745–2788, 2012
www.geosci-model-dev-discuss.net/5/2745/2012/
doi:10.5194/gmdd-5-2745-2012

Geoscientific Model Development Discussions

Modeling atmospheric ammonia and ammonium using a backward-in-time stochastic Lagrangian air quality model (STILT-Chem v0.7)

D. Wen[1], J. C. Lin[1,2], L. Zhang[3], R. Vet[3], and M. D. Moran[3]

[1]Waterloo Atmosphere-Land Interactions Research Group, Department of Earth and Environmental Sciences, University of Waterloo, USA
[2]Department of Atmospheric Sciences, University of Utah, USA
[3]Air Quality Research Division, Science and Technology Branch, Environment Canada, Canada

Received: 10 July 2012 – Accepted: 24 August 2012 – Published: 12 September 2012

Correspondence to: D. Wen (dwen@uwaterloo.ca)

Published by Copernicus Publications on behalf of the European Geosciences Union.

Abstract

A new chemistry module of atmospheric ammonia (NH_3) and ammonium (NH_4^+) was incorporated into a backward-in-time stochastic Lagrangian air quality model (STILT-Chem) that was originally developed to simulate the concentrations of a variety of gas-phase species at receptors. STILT-Chem simulates the transport of air parcels backward in time using ensembles of fictitious particles with stochastic motions, while simulating emissions, deposition and chemical transformation forward in time along trajectories identified by the backward-in-time simulations. The incorporation of the new chemistry module allows the model to simulate not only gaseous species, but also multi-phase species involving NH_3 and NH_4^+. The model was applied to simulate concentrations of NH_3 and particulate NH_4^+ at six sites in the Canadian province of Ontario for a six-month period in 2006. The model-predicted concentrations of NH_3 and particulate NH_4^+ were compared with observations, which show broad agreement between simulated concentrations and observations. Since the model is based on back trajectories, the influence of each major process such as emission, deposition and chemical conversion on the concentration of a modeled species at a receptor can be determined for every upstream location at each time step. This makes it possible to quantitatively investigate the upstream processes affecting receptor concentrations. The modeled results suggest that the concentrations of NH_3 at those sites were significantly and frequently affected by southwestern Ontario, northern Ohio, and nearby areas. NH_3 is mainly contributed by emission sources whereas particulate NH_4^+ is mainly contributed by the gas-to-aerosol chemical conversion of NH_3. Dry deposition is the largest removal process for both NH_3 and particulate NH_4^+. This study revealed the contrast between agricultural versus forest sites. Not only were emissions of NH_3 higher, but removal mechanisms (especially chemical loss for NH_3 and dry deposition for NH_4^+) were less efficient for agricultural sites. This combination explains the significantly higher concentrations of NH_3 and particulate NH_4^+ observed at agricultural sites.

GMDD
5, 2745–2788, 2012

1 Introduction

Ammonia (NH_3) is the primary basic gas in the atmosphere. NH_3 acts as a major agent in neutralizing acids in the atmosphere and plays an important role in aerosol formation. Thus NH_3 has major impacts on human health, acid deposition, atmospheric visibility, and radiative forcing. The significant sources of NH_3 are animal waste, ammonification of humus followed by emission from soils, losses of NH_3-based fertilizers from soils, and industrial emissions (Asman et al., 1998). In the atmosphere, NH_3 is subject to transport and diffusion, removal by dry and wet deposition, and transformation to aerosol-bound NH_4^+ in reactions with acid gases and aerosols. Excessive deposition of atmospheric NH_3 and NH_4^+ may lead to soil acidification and damage to sensitive species and ecosystem health (Van Bremen et al., 1982; Morris, 1991).

Measurements of NH_3 and NH_4^+ concentrations from monitoring programmes not only provide information about actual levels and trends of NH_3 in the environment, but also form the basis of our understanding of the physical and chemical processes governing the fate of NH_3. However, measurements alone are usually insufficient for a complete understanding of those processes due to the limited number of monitoring locations and the inability to observe processes of interest as an air parcel is advected over the landscape. Modeling atmospheric NH_3 yields additional insights by providing information about locations not covered by the monitoring network as well as processes that are not measured explicitly. Well-tested and validated air quality models are thus highly useful in the assessment and interpretation of ambient NH_3 and NH_4^+ measurements.

The main goals of this study are: (1) to develop a stochastic back-trajectory based air quality model for simulating atmospheric NH_3; (2) to use this model to interpret NH_3 and particulate NH_4^+ (p-NH_4^+) concentrations at monitoring sites; (3) to quantitatively assess the contributions of various sources, sinks, and processes to the sites.

GMDD
5, 2745–2788, 2012

2 Model description

The model used in this study is a backward-in-time stochastic Lagrangian air quality model (STILT-Chem) (Wen et al., 2012), was built from the Stochastic Time-Inverted Lagrangian Transport model (STILT; see http://www.stilt-model.org) (Lin et al., 2003), which in turn was based on the HYbrid Single-Particle Lagrangian Integrated Trajectory (HYSPLIT) model (Draxler and Hess, 1997). STILT-Chem is an effective tool to investigate the upstream influences of emission, deposition and chemical conversion on receptors. The simulation of the model begins with a stochastic back-trajectory simulation, followed by forward calculations that determine tracer concentrations along the generated back trajectories (Wen et al., 2012). In the back-trajectory simulation, numerous particles, each representing an air parcel, are released from a receptor and transported backward in time for a specific period. Each particle is transported by both interpolated mean wind fields as well as stochastic velocities representing turbulent eddies. After back trajectories are calculated, the concentrations of modeled species are initialized at the endpoint of each back trajectory using values output from a global chemical transport model (Sect. 3.2.1). The initial parcel concentrations are then evolved forward in time along each trajectory to take into consideration the influences of emissions, deposition, mixing, and chemical transformation. Although the STILT-Chem model is capable of simulating a variety of gas-phase species in the atmosphere using the Carbon Bond IV (CB4) mechanism (Gery et al., 1989), atmospheric NH_3 was originally omitted by the CB4 due to the involvement of multi-phase reactions in its dominant atmospheric chemical processes. In this study, we have added an additional chemistry module into STILT-Chem, allowing it to simulate atmospheric NH_3 and particulate NH_4^+, in addition to the original CB4-related gas-phase species. The treatment of transport and diffusion, emissions, deposition, and chemistry for the CB4 species in the model has been described thoroughly by Wen et al. (2012). Hence in this paper a detailed and comprehensive description is only presented for the new implementation of NH_3 and NH_4^+ and an alternative dry deposition scheme in STILT-Chem.

GMDD
5, 2745–2788, 2012

2.1 Transport and diffusion

The STILT-Chem model simulates the transport of air parcels, represented as fictitious particles, backward in time. Each fictitious particle is advected with mean wind velocities as well as stochastic velocities parameterized to represent the effect of turbulent transport. The effect of the turbulence is simulated by adding a random velocity to the mean motion for each particle. This random velocity is a function of the turbulence intensity and is different for each particle. Turbulent strengths were diagnosed from meteorological fields (Sect. 3.2) using the Hanna scheme (Hanna, 1982). The detailed treatment of transport and diffusion in the model can been found in Lin et al. (2003) and Draxler and Hess (1997).

2.2 Emissions

The molar mixing ratio change of a species in a particle due to surface emissions is calculated using a "footprint" concept and emission fluxes. A footprint $f(\boldsymbol{x}_\mathrm{r}, t_\mathrm{r}|x_i, y_j, t_m)$, in units of ppm $(\mu\mathrm{mole\,m^{-2}\,s^{-1}})^{-1}$, which is calculated in a back-trajectory simulation, represents the sensitivity of the molar mixing ratio arriving at its receptor at location $\boldsymbol{x}_\mathrm{r}$ at time t_r to the surface flux $F(x_i, y_j, t_m)$ from location x_i, y_j at time t_m (Lin et al., 2003; Wen et al., 2012, 2011). Thus it is a measure of the contribution from a source of unit strength located at x_i, y_j at time t_m to the mixing ratio at the receptor. The footprint is derived from the local density of particles by counting the number of particles (out of total number N_tot) in surface-influenced boxes and determining the amount of time $\Delta t_{p,i,j,k}$ each particle p spends in each surface volume element (i, j, k) during each time step. The mathematical definition of a footprint (Lin et al., 2003) is given by:

$$f(\boldsymbol{x}_\mathrm{r}, t_\mathrm{r}|x_i, y_j, t_m) = \frac{m_\mathrm{air}}{h\bar{\rho}(x_i, y_j, t_m)} \frac{1}{N_\mathrm{tot}} \sum_{p=1}^{N_\mathrm{tot}} \Delta t_{p,i,j,k} \quad (1)$$

GMDD
5, 2745–2788, 2012

where m_{air} is the molar mass of air, h is the height below which turbulent mixing is strong enough to mix the surface flux thoroughly, and $\bar{\rho}(x_i, y_j, t_m)$ is the average air density below h.

The molar mixing ratio change $\Delta Q_{s,p}(\boldsymbol{x}_r, t_r | x_i, y_j, t_m)$ of the s-th species in the p-th particle arriving at its receptor at time t_r due to a surface emission flux $F(x_i, y_j, t_m)$ (μmole m^{-2} s^{-1}) is incremented whenever the parcel dips below a specific height h, which is determined in STILT as a fraction of the PBL height (Lin et al., 2003). The fraction was set to 0.5 in this study. The mixing ratio change at the receptor is given by:

$$\Delta Q_{s,p}(\boldsymbol{x}_r, t_r | x_i, y_j, t_m) = f(\boldsymbol{x}_r, t_r | x_i, y_j, t_m) F(x_i, y_j, t_m) \tag{2}$$

This footprint formulation is applied for emissions at the surface. For emissions at altitude (e.g., smokestacks) we dilute the emission throughout the grid box in which the higher altitude emission is found. So the mixing ratio change at the receptor for an emission at altitude is given as follows (Wen et al., 2011):

$$\Delta Q_{s,p}(\boldsymbol{x}_r, t_r | x_i, y_j, z_k, t_m) = \frac{D(x_i, y_j, z_k, t_m)}{N_{\text{tot}}} \sum_{p=1}^{N_{\text{tot}}} \Delta t_{p,i,j,k}$$

$$= F(x_i, y_j, z_k, t_m) \frac{m_{\text{air}}}{\Delta z \bar{\rho}(x_i, y_j, z_k, t_m)} \frac{1}{N_{\text{tot}}} \sum_{p=1}^{N_{\text{tot}}} \Delta t_{p,i,j,k}. \tag{3}$$

where $F(x_i, y_j, z_k, t_m)$ is the emission flux in a grid box (i, j, k) at time t_m. $D(x_i, y_j, z_k, t_m)$ represents the dilution of emission flux in the grid box with a thickness of Δz. Molar mixing ratios (ppm) are converted into concentrations (μg m^{-3}) afterwards by multiplying with air density. Details concerning the North American emissions that were used in this study are provided in Sect. 3.2.2.

GMDD
5, 2745–2788, 2012

2.3 Gas-phase chemistry for CB4 species

The CB4 gas-phase chemistry mechanism (Gery et al., 1989) is used in the model to simulate chemical transformations for gas-phase species. The CB4 mechanism was originally developed primarily to simulate urban and regional ozone formation and is a collection of gas-phase reactions that transform reactants into products, including key intermediates. The mechanism used here is a modified version that contains 92 reactions involving 38 chemical species (Stein et al., 2000). The differential equations of this mechanism are solved using a modified Gear method (Gear, 1971; Press et al., 1992; Spellmann and Hindmarsh, 1975). The photolysis rate constants required to calculate the chemical transformations are computed as a function of the solar zenith angle, cloud cover, and chemical species for each particle at each time step. NH_3 is not included in the standard CB4 mechanism.

2.4 Implementing chemistry for NH_3 and NH_4^+

NH_3 can react with O_2, HCl, OH radical, nitric acid vapor, and sulfuric acid in the atmosphere. However, not all gas-phase reactions of NH_3 are important (Seinfeld and Pandis, 2006) due to either small reaction constants or low concentrations of reactants. The dominant reactions of NH_3 in the atmosphere are with nitric acid vapor and sulfuric acid (Seinfeld and Pandis, 2006). Thus only reactions with nitric acid vapor and sulfuric acid are considered in this study.

2.4.1 Reaction with H_2SO_4

$$NH_3 + H_2SO_4 \rightarrow NH_4HSO_4(s) \quad \text{(R1)}$$

$$NH_3 + NH_4HSO_4(s) \rightarrow (NH_4)_2SO_4(s) \quad \text{(R2)}$$

If sulfuric acid (H_2SO_4) is present in the atmosphere, gaseous NH_3 will practically always react with H_2SO_4 in either gas or aerosol phase. This process is considered

GMDD
5, 2745–2788, 2012

irreversible. NH_3 is expected to react instantaneously to fully neutralize the available H_2SO_4. The formation of ammonium sulfate ($(NH_4)_2SO_4$) and ammonuim bisulfate (NH_4HSO_4) is thus only limited by the availability of either NH_3 or H_2SO_4. For simplicity, an equal mixture of $(NH_4)_2SO_4$ and NH_4HSO_4 was assumed for ammonium sulfate production from this reaction (EMEP, 1998) in the model, although more complex inorganic thermodynamic equilibrium schemes do not make this assumption (Nenes et al, 1999; Wexler and Clegg, 2002).

The availability of H_2SO_4 is mainly determined by its emissions, deposition, and chemical conversions. The formation of H_2SO_4 from gas-phase chemical processes is calculated by the CB4 mechanism. The major aqueous-phase formation is from the conversion of dissolved SO_2 and is estimated following an approach from Rolph et al. (1992, 1993).

When SO_2 dissolves in water, three species are formed: H_2SO_3, HSO_3^-, and SO_3^{2-}. These three species can be oxidized by hydrogen peroxide (H_2O_2), O_3, OH^-, or O_2 in the presence of catalysts (Fe^{3+}, Mn^{2+}). However, only the oxidation by H_2O_2 is the most important (Hoffmann and Calvert, 1985) when pH ≤ 5. Since this is a common pH value of rain water (Charlson and Rodhe, 1982), we assume that this oxidation reaction is the only aqueous-phase reaction affecting sulfuric acid production from dissolved SO_2. Thus, the concentration changes of gaseous SO_2 and aqueous sulfuric acid due to the aqueous-phase oxidation of dissolved SO_2 can be determined as (Rolph et al., 1992):

$$-\frac{d[SO_2]}{dt} = k_w[SO_2] \quad (4)$$

and

$$\frac{d[(SO_4^{2-})_w]}{dt} = k_w[SO_2] \quad (5)$$

where the rate constant k_w is a function of the air concentration of H_2O_2, the liquid water content in the cloud (L), and the air concentration of SO_2.

$$k_w = 41.57L[H_2O_2]e^{-0.233[SO_2]} \quad (6)$$

GMDD
5, 2745–2788, 2012

The air concentration of H_2O_2 required in Eq. (6) is computed and provided by the CB4 mechanism. L is set to 0.9 g m^{-3}.

2.4.2 Reaction with HNO_3

In the atmosphere, NH_3 and HNO_3 vapor can react to form ammonium nitrate (NH_4NO_3) under conditions when excess NH_3 is available after reacting with H_2SO_4.

$$NH_3(g) + HNO_3(g) \rightleftharpoons NH_4NO_3(s, aq) \quad \text{(R3)}$$

This is a major route of NH_3 to form particle nitrate. The production of this reaction, controlled by the ambient temperature (T) and relative humidity (RH), may exist as a solid or as an aqueous solution.

NH_4NO_3 exists as a solid if RH is less than the deliquescence relative humidity (RH_d) (Mozurkewich, 1993):

$$\ln RH_d = \frac{618.3}{T} - 2.551 \quad (7)$$

where RH_d is a fraction and T is in Kelvins. The corresponding equilibrium reaction is

$$NH_3(g) + HNO_3(g) \rightleftharpoons NH_4NO_3(s) \quad \text{(R4)}$$

The dissociation constant $K_p(T)$ of the Reaction (R4) is equal to the product of the partial pressures of NH_3 and HNO_3, and can be determined by (Mozurkewich, 1993):

$$\ln K_p = 118.87 - \frac{24084}{T} - 6.025 \ln(T) \quad (8)$$

The equilibrium constant K_{eq} of the Reaction (R4), in this case, is equal to K_p.

If RH is greater than RH_d, NH_4NO_3 will be in the aqueous state. The corresponding dissociation reaction is then

$$NH_3(g) + HNO_3(g) \rightleftharpoons NH_4^+ + NO_3^- \quad \text{(R5)}$$

GMDD
5, 2745–2788, 2012

In this case, the equilibrium constant, $K_{eq}(T)$, is given by (Mozurkewich, 1993):

$$K_{eq} = [P_1 - P_2(1 - \frac{RH}{100}) + P_3(1 - \frac{RH}{100})^2](1 - \frac{RH}{100})^{1.75} K_p \quad (9)$$

where both K_p and K_{eq} are in units of $(\text{molecules cm}^{-3})^2$ and RH is in percent. P_1, P_2 and P_3 are calculated as follows (Mozurkewich, 1993):

$$\ln P_1 = -135.94 + \frac{8763}{T} + 19.12 \ln(T) \quad (10)$$

$$\ln P_2 = -122.65 + \frac{9969}{T} + 16.22 \ln(T) \quad (11)$$

$$\ln P_3 = -182.61 + \frac{13875}{T} + 24.46 \ln(T) \quad (12)$$

Equilibrium concentrations of gaseous NH_3 and HNO_3, and the resulting concentration of solid or aqueous NH_4NO_3, are calculated from fundamental thermodynamic principles. The equilibrium concentration of NH_3 is given by the Equation (EMEP, 1998):

$$[NH_{3eq}] = \frac{[NH_3] + [HNO_3]}{2} + \sqrt{\frac{([NH_3] - [HNO_3])^2}{4} + K_{eq}} \quad (13)$$

The air concentration of HNO_3 from gas-phase chemical reactions is calculated by the CB4 mechanism. Heterogeneous conversion of N_2O_5 to HNO_3 on the surface of aerosol particles that contain water is not included in the model. The contribution of this process to the air concentration of HNO_3 is therefore neglected.

GMDD
5, 2745–2788, 2012

2.5 Deposition

The concentration change of the s-th species due to dry and wet deposition is expressed in terms of time constants:

$$\frac{dC_s}{dt} = -(\beta_{d_s} + \beta_{w_s})C_s \quad (14)$$

where β_{d_s} and β_{w_s} are time constants for dry and wet deposition for the s-th species, respectively.

2.5.1 Dry deposition

The time constant for dry deposition is expressed as follows:

$$\beta_{d_s} = \frac{V_{dry_s}}{Z_s} \quad (15)$$

Dry deposition is only estimated when a particle moves into the lowest model level, the depth of which (Z_s) is approximately 50 m in this study and which is assumed to be the top of the surface layer. V_{dry_s} (cm s^{-1}) is the dry deposition velocity for the s-th species. The dry deposition velocities of all modeled species (including gas-phase CB4 species, NH_3, particulate NH_4^+, NO_3^-, and SO_4^{2+}) can be either calculated or provided explicitly.

A dry deposition scheme based on the work of Wesely (1989) was used originally by the model to calculate dry deposition velocities for the modeled gaseous and aerosol species (Draxler and Hess, 1997).

In this study, we added another dry deposition approach developed by Zhang et al. (2001, 2003) (hereafter referred to as the "Zhang approach") as another option to calculate dry deposition velocities for the modeled species. The Zhang approach calculates dry deposition velocities for more than 30 gaseous species and 14 particulate

GMDD
5, 2745–2788, 2012

species that are usually considered in air quality models. Although it employs a similar approach used in Wesely (1989), the Zhang approach incorporates vegetation density effects via leaf area index and possesses an updated representation of non-stomatal deposition pathways, including improved treatment of snow cover. In this approach, dry deposition is parameterized as a species-specific weighted combination of the deposition properties of two archetypal species: O_3 and SO_2. Non-stomatal resistance (including in-canopy aerodynamic resistance, soil resistance, and cuticle resistance) for SO_2 and O_3 is parameterized as a function of friction velocity, relative humidity, leaf area index, and canopy wetness. Non-stomatal resistance for all other species is scaled to those of SO_2 and O_3 based on their chemical and physical characteristics. Dry deposition of particulate species is calculated as a function of particle size (Zhang et al., 2001). The Zhang approach is formulated for 26 land-use categories and widely used by air quality models such as GEOS-chem (Alexander et al., 2005), the Comprehensive Air quality Model with Extensions (CAMx) (Nopmongcol et al, 2012), and A Unified Regional Air-quality Modelling System (AURAMS) (Zhang et al., 2002).

2.5.2 Wet deposition

Wet deposition is represented via loss rates computed based on precipitation rates. The wet deposition velocity for the *s*-th gas-phase species can be calculated as (Draxler and Hess, 1997):

$$V_{\mathrm{wet}_s} = H_s \mathrm{RTP} \tag{16}$$

where H_s is the effective Henry's Law constant of the *s*-th species, R is the universal gas constant ($0.082\,\mathrm{atm\,mol^{-1}\,K^{-1}}\,L$), and T and P are, respectively, air temperature and precipitation rate in an air parcel. The gaseous wet removal time constant is given by:

$$\beta_{\mathrm{w}_s} = \frac{F_{\mathrm{t}} V_{\mathrm{wet}_s}}{Z_p} \tag{17}$$

GMDD
5, 2745–2788, 2012

where Z_p is the depth of the meteorological layer in which the particle is found. F_t is the fraction of the layer that is below cloud top. Wet removal of all modeled gas-phase species except for SO_2 was calculated using this equation.

Wet deposition of SO_2 was determined following a method from Rolph et al. (1992):

$$SO_{2(aq)} = \frac{AL}{1 + AL} SO_{2(g)} \quad (18)$$

where A is a constant equal to 0.0533. L is the liquid water content and set to 0.9 g m^{-3}. SO_2(g) is the air concentration of SO_2.

Particulate SO_4^{2-} in cloudwater consists of the SO_4^{2-} particles acting as condensation nuclei and the SO_4^{2-} formed by aqueous oxidation. The in-cloud content of particulate SO_4^{2-} can be expressed as (Rolph et al., 1992):

$$(SO_4^{2-})_{ic} = \alpha (SO_4^{2-})_d + (SO_4^{2-})_w \quad (19)$$

where α = 0.65, an empirical factor, is the ratio of the activated particles to the total number of SO_4^{2-} particles. $(SO_4^{2-})_d$ is the SO_4^{2-} air content due to gas-phase oxidation and emissions. $(SO_4^{2-})_w$ is the amount of SO_4^{2-} formed by aqueous-phase oxidation and is calculated by:

$$\frac{d[(SO_4^{2-})_w]}{dt} = k_w [SO_2] \quad (20)$$

where k_w is given in Eq. (6).

The wet removal of SO_4^{2-} within cloud is given by (Rolph et al., 1992, 1993):

$$(SO_4^{2-})_{pp} = \lambda (SO_4^{2-})_{ic} \quad (21)$$

where $\lambda = (18P)^{1/2}$ is the scavenging ratio, representing the ratio of the SO_4^{2-} removed by precipitation to the SO_4^{2-} content in the cloud, and P is the precipitation rate in m h^{-1}.

GMDD
5, 2745–2788, 2012

For particulate NH_4^+ and NO_3^-, wet deposition velocity within cloud is computed as the product between scavenging ratio S and precipitation rate P:

$$V_{inc} = SP \tag{22}$$

Different scavenging ratios can be defined for different pollutants. In this work we used 3.1×10^5 for particulate NH_4^+ and 4.9×10^5 for particulate NO_3^- (Hicks, 2005). The time constant for within-cloud removal is:

$$\beta_{inc} = \frac{F_t F_b V_{inc}}{Z_p} \tag{23}$$

where F_b, similar to F_t, is the fraction of the layer that is above cloud bottom.

Below-cloud removal for particulate NH_4^+ and NO_3^- is defined directly as a rate constant, independent of the precipitation rate (Draxler and Hess, 1997):

$$\beta_{bel} = 5 \times 10^{-5}(1.0 - F_b) \tag{24}$$

The below-cloud scavenging of particulate SO_4^{2-} by falling droplets is expressed as (Rolph et al., 1992, 1993):

$$\frac{-d(SO_4^{2-})}{dt} = k'_{wd}(SO_4^{2-})_d \tag{25}$$

where $k'_{wd} = 1 \times 10^{-4}\ h^{-1}$, the rate of wet removal of SO_4^{2-}, is a function of raindrop and particle size distributions. An average size for both distributions is assumed.

3 Measurement and model simulation

3.1 Measurement sites used for simulation and comparison

Six measurement sites of NH_3 and p-NH_4^+ in Ontario, Canada, were selected as receptors in the model simulations (Fig. 1). Details regarding the six sites can be found

GMDD
5, 2745–2788, 2012

in Table 1. The measurements of NH_3 were carried out during the Southern Ontario Ammonia Passive Sampler Survey (SOAPSS) (Vet et al., 2008), which ran from 4 April 2006 to 27 March 2007. The objective of the survey was to measure concentrations of ambient NH_3 at approximately 78 sites in southern Ontario and a small number of Canadian sites outside of Ontario and US sites in the states along the Great Lakes.

The NH_3 measurements represent an integrated average of the NH_3 concentration over a one-week (before December, 2006) or two-week (after November, 2006) period at the six selected sites – Longwoods, Egbert, Sprucedale, Chalk River, Haliburton, and St. Mary's – using passive samplers. Of these six sites, p-NH_4^+ concentrations were also measured over 24-h periods by the Canadian Air and Precipitation Monitoring Network (CAPMoN) at four sites – Chalk River, Egbert, Longwoods, and Sprucedale – using a filter-pack system (Sirois, 1997; Zhang et al, 2008). The six sites can be grouped into two categories based on local land use: agriculture and forest (Table 1). These sites were selected mainly to investigate the differences of NH_3 and p-NH_4^+ between these two categories in southern Ontario.

3.2 Simulation setup

The model was used to simulate NH_3 and p-NH_4^+ hourly concentrations at the six sites shown in Fig. 1 for half a year, from 1 June to 30 November 2006. The simulations were driven by meteorological data from the US NCEP's North American Regional Reanalysis (NARR) (Mesinger et al, 2006). The NARR meteorological fields have 349×277 gridcells with a grid spacing of 32 km covering all of North America on a Lambert Conformal Conic projection in three-hourly intervals. The dataset has 45 vertical layers, including 29 pressure layers from the surface up to 100 hPa, 5 subsurface layers, and other monolevels. The lowest five pressure layers were set to 1000, 975, 950, 925, and 900 hPa, respectively. Except for cloud levels, incident solar radiation, boundary layer depth, turbulent intensity, cloud bottom/top, which are computed by the STILT-Chem model, all other meteorological variables required by the model are available in NARR. In the simulations, ensembles of 500 particles were released

GMDD
5, 2745–2788, 2012

every hour from each site location at a height of 5 m above ground. The choice of 500 particles will be explained in Sect. 4.1. These particles were run backward in time for six days, which usually allowed them to travel far away from any sources near the receptors. Dynamic integration time steps were used for the back-trajectory calculation. They were computed from the requirement that the advection distance per time-step should be less than the grid spacing (Courant-Friedrichs-Lewy condition). The same time steps computed for the back-trajectory transport calculation were also used in the forward simulation for deposition and chemistry calculations. Dry deposition velocities of modeled species were calculated using the Zhang approach.

3.2.1 Initial/boundary conditions

Concentrations of modeled species were initialized at the endpoints of trajectories using the output of the Model for OZone And Related chemical Tracers, version 4 (MOZART-4) (Emmons et al., 2010), according to the temporal and spatial locations of trajectory endpoints in the MOZART-4 simulation output. MOZART-4 (http://www.acd.ucar.edu/gctm/mozart/models/m4/) is a global chemical transport model which is driven by NCEP/NCAR-reanalysis meteorology and uses emissions based on the Precursors of Ozone and their Effects in the Troposphere (POET) database (Granier et al, 2005), the Regional Emission inventory for Asia (REAS) (Ohara et al, 2007), and the Global Fire Emissions Database version 2 (GFED2) (van der Werf et al, 2006). MOZART-4 output for 2006 was obtained from the WRF-Chem website (http://www.acd.ucar.edu/wrf-chem/mozart.shtml) for particle initialization in this study. The output has a $2.8^{\circ} \times 2.8^{\circ}$ horizontal resolution with 28 vertical levels from the surface to approximately 2 hPa, in a 6-h time interval. Since chemical species in the output of MOZART-4 are different from those of CB4, chemical species in the output were approximately mapped onto CB4 species according to the matching table given by Emmons et al. (2010). After the initialization, the simulation is performed forward in time to simulate the evolution of concentration due to the influences of emission, chemical reactions and deposition along each trajectory for each time step.

GMDD
5, 2745–2788, 2012

3.2.2 Emissions datasets and processing

The Canadian emissions inventory that was used for this study was the 2006 Canadian Criteria Air Contaminants emissions inventory (version 2) from Environment Canada (EC), which incorporates facility-level emissions from the EC National Pollutant Release Inventory plus province-level estimates of on-road mobile emissions, off-road mobile emissions, and area emissions (http://www.ec.gc.ca/inrp-npri/). A special inventory of 2006 Canadian agricultural NH_3 emissions that was developed under the Canadian National Agri-Environmental Standards Initiative (NAESI) was also used (Makar et al, 2009). The corresponding US and Mexican emissions inventories were the 2005 US National Emissions Inventory (version 4) and the 1999 Mexican emissions inventory. Both were obtained from the US Environmental Protection Agency (http://www.epa.gov/ttn/chief/eiinformation.html). These inventories include emissions for oxides of nitrogen (NO_x), VOC, NH_3, carbon monoxide (CO), oxides of sulphur (SO_x), and primary particulate matter (PM) with an aerodynamic diameter less than or equal to 10 µm and 2.5 µm (PM_{10} and $PM_{2.5}$). More information about these inventories may be found in Pouliot et al. (2012).

The hourly anthropogenic gridded emissions fields used in this study were prepared using the Sparse Matrix Operator Kernel Emission (SMOKE) (v2.4) (UNC, 2009) emissions processing system for a domain (Fig. 1) that consists of 150 × 106 gridcells with a horizontal grid spacing of 42 km on a secant polar stereographic projection true at 60° N. For simplicity all point sources were treated as surface sources, which is reasonable for NH_3 emissions. We also incorporated the Models-3 Input/Output Application Programming Interface (IOAPI) (Coats, 2003) into the model to read in emissions fields directly from SMOKE output files.

GMDD
5, 2745–2788, 2012

4 Results

4.1 Sensitivity to particle number

Due to the stochastic nature of particle (air parcel) trajectories, the accuracy of STILT-Chem is affected by the number of particles used. Theoretically, an infinite number of particles are required to completely represent the ensemble properties of transport to a given measurement location. In reality, however, only a finite number of particles can be simulated due to limited computational resources. This leads to incomplete sampling of trajectory pathways and emissions, resulting in fluctuations in simulated concentrations.

To find the appropriate number of particles in a simulation that can achieve adequate accuracy while also reducing the computational cost, we ran the model with different particle numbers for the Egbert measurement site for ten days. The particle numbers examined included 10, 50, 100, 500, 1000, 2000 and 3000, and simulated NH_3 and p-NH_4^+ concentration time series are presented in Fig. 2. The results show that simulated concentrations with a small particle number are more variable than those with a large number. Discrepancies between simulations with small and large numbers of particles are significant. When the particle number is larger than 500, however, modeled concentrations converge on the modeled values with 3000 particles and almost overlap with each other. Therefore, we assumed that the modeled results with 3000 particles act like "true values" without error caused by insufficient particles. Figure 2 also shows the deviations of all simulations relative to the simulation with 3000 particles, where the discrepancy is calculated as the Mean Normalized Gross Error (MNGE, defined in Table 2). Since the model run time is proportional to the number of particles, we chose 500 particles for use in the present simulations, which yielded an MNGE less than 5 % for both NH_3 and p-NH_4^+ compared to a run with 3000 particles.

GMDD
5, 2745–2788, 2012

4.2 Model performance

4.2.1 NH_3

Simulated hourly NH_3 concentrations were averaged over each corresponding sampling weekly period and then compared against measurements for all six receptor sites for the simulation period from 1 June to 30 November 2006. The weekly time series shown in Fig. 3 suggest that the model generally performed adequately in predicting the average levels of NH_3 observations for most sites, especially for the three sites in forest regions – Sprucedale, Haliburton, and Chalk River. However, the week-to-week variations of the observations were not well captured by the model. The NH_3 concentrations at Longwoods, Egbert, Chalk River, and Haliburton were overestimated, whereas those at St. Mary's and Sprucedale were underestimated (see Table 3). The overestimation at Longwoods and underestimation at St. Mary's may indicate that coarse representation (i.e., 42 km grid spacing) and/or uncertainties in emissions contribute to the underestimation and overestimation of NH_3 because emission strengths between those two sites are not significantly different (Fig. 1). There is no indication, on the other hand, of significant overall overestimation or underestimation of NH_3 by the model. The better performance of the model for the three sites in the forest region is probably due to the smaller emission fluxes and weaker spatial gradients in their vicinity as compared with the three sites in the agricultural region.

The correlation between measured and modeled concentrations is another frequently used model performance metric. We calculated the correlation between the modeled and measured NH_3 concentrations for all test sites and obtained a value of 0.807 (Fig. 4a). The figure also shows that most calculated concentrations agreed, within a factor of 2, with observed concentrations. Given that NH_3, like SO_2 and NO_x, is a primary pollutant and has strong spatial variability, NH_3 is generally more difficult for air quality models to simulate than secondary pollutants such as $p\text{-}NH_4^+$ and O_3. So far, no criteria have been recommended for model performance in NH_3 modeling, largely due to the paucity of available NH_3 measurement data. In fact, the SOAPSS

GMDD
5, 2745–2788, 2012

data of NH_3 measurements from a network of sites was the first such data set available for North America. As a result, we cannot compare model performance for NH_3 in this study with results for other models.

4.2.2 $p\text{-}NH_4^+$

Hourly simulated $p\text{-}NH_4^+$ concentrations were averaged to daily concentrations to match the CAPMoN filter-pack sampling period. Time series of daily measured and modeled $p\text{-}NH_4^+$ concentrations for four of the receptor sites are presented in Fig. 5. Two sites, St. Mary's and Haliburton, were not included due to their lack of $p\text{-}NH_4^+$ measurements. Qualitatively, we can see that the model, in most cases, can simulate the synoptic variations, the timing of the peaks, and the mean levels of the measurements.

Model performance for $p\text{-}NH_4^+$ was also evaluated with measurements for those four sites using two model performance metrics recommended by Boylan and Russell (2006) and US EPA (2007) for aerosols: the mean fractional bias (MFB) and the mean fractional error (MFE), along with the ratio of the means (ROM) and the unpaired peak accuracy (UPA). Their definitions are listed in Table 2. MFB and MFE indicate the overall performance of the model while UPA represents the model's ability to simulate the peak concentrations. As indicated in Table 3, all MFBs and MFEs for $p\text{-}NH_4^+$ meet the acceptable model performance criteria ($MFE \leq 75\,\%$ and $-60\,\% < MFB < 60\,\%$) suggested by Boylan and Russell (2006). All of the values are also comparable to values reported by other studies (Aksoyoglu et al., 2011; Appel et al., 2008; Tesche et al., 2006), indicating satisfactory performance of the model in simulating $p\text{-}NH_4^+$. Ratio-of-the-means (ROM) values presented in Table 3 indicate that the model predicted means of $p\text{-}NH_4$ measurements very well, with a 2 % to 8 % over-prediction. One of the possible causes of the over-prediction is that the CAPMoN $p\text{-}NH_4^+$ observations measured by a filter-pack system are likely to be lower than actual values because captured NH_4NO_3 can be subject to volatility issues (Cheng and Tsai, 1997; Zhang and McMurry, 1987). The statistics in Table 3 also show that there is no significant difference in model performance between sites in agricultural regions (Egbert and Longwoods)

GMDD
5, 2745–2788, 2012

and those in forest regions (Sprucedale and Chalk River) for $p\text{-}NH_4^+$ simulations, in part because $p\text{-}NH_4^+$, unlike NH_3, is a secondary (regional) pollutant and has smaller spatial gradients.

Lastly, Fig. 4b shows a combined scatterplot of daily $p\text{-}NH_4^+$ values for the four receptor sites with measurements. The calculated correlation was 0.59. This value is comparable with other studies that used forward-in-time Eulerian air quality models, such as a 0.76 correlation obtained for the AURAMS model for a one-year 2002 simulation (Makar et al, 2009) and values ranging from 0.58 to 0.84 obtained by the CMAQ model for different months of 2001 (Appel et al., 2008).

4.3 Quantitative identification of upstream influences

4.3.1 Identification of important upstream locations

Since the STILT-Chem model is back-trajectory-based, the evolution of concentrations of modeled species can be calculated along each trajectory during every time step, for each process involved. This allows us to investigate upstream processes affecting concentrations at specified receptors. Figure 6, for an example, shows calculated NH_3 concentration changes in upstream areas caused by different processes, obtained by averaging within each grid cell the values associated with different trajectories. Those calculated values directly determine the concentration of NH_3 arriving at Egbert at 18:00 (GMT) on 2 July 2006. Figure 6b shows emission contribution average to Egbert at the specified time from each source gridcell, derived by multiplying the footprint (Fig. 6a) with the emission map. Figure 6d, e and f presents contributions averages for each gridcell from dry deposition, chemical conversion, and wet deposition, respectively.

First, the calculated footprint (Fig. 6a; cf. Sect. 2.2) shows the main air flows that affect the level of NH_3 simulated at Egbert at that time. Combined with emission fluxes (see Eq. 2), those values of footprints can be applied to determine concentration changes contributed by emissions for every upstream location (Fig. 6b). The

GMDD
5, 2745–2788, 2012

modeled dry deposition velocities of NH_3 are shown in Fig. 6c for every upstream location, which mainly vary from 0.1 to 4.0 cm s^{-1}. The upstream locations where NH_3 was significantly removed by dry deposition can be identified (Fig. 6d) by combining those dry deposition velocities and ambient NH_3 concentrations in their corresponding locations (cf. Sect. 2.5.1). High loss of NH_3 due to chemical conversion in some upstream locations (Fig. 6e) was probably caused by the presence of H_2SO_4 or HNO_3 associated with SO_2 and NO_x emissions upwind of those locations. Wet removal of NH_3 is highly localized and dependent on precipitation rates in the upstream regions (Fig. 6f).

The results presented in Fig. 6 are only useful for investigating upstream sources or sinks influencing the receptor at one time. However, the same analyses can be averaged over a long time period to identify upstream sources and sinks that impact receptors significantly. As an example, the upstream NH_3 concentration changes caused by different processes – such as emissions, dry deposition, wet deposition and chemical conversion – were calculated for each simulation hour (e.g., Fig. 6), and were then averaged over the entire six-month simulation period. The resulting values are displayed in Fig. 7 for two sites, Longwoods and Chalk River, with very different characteristics (Fig. 1).

As noted earlier, Longwoods is representative of sites associated with extensive local agricultural operations and near strong NH_3 sources while Chalk River is a forested site surrounded by low emissions strengths. Figure 7 clearly shows that NH_3 concentrations were enhanced (represented in red color) in the upstream areas due to emissions. Contributions from different upstream locations also differ significantly. On a time scale of 6 months, the main source regions that impact Longwoods and Chalk River are located in southwestern Ontario in Canada and the northern part of Ohio, in the US. However, the magnitude of the emission contributions of these areas to Longwoods is much higher than to Chalk River. This helps explain why the simulated and measured NH_3 concentrations at Longwoods are much higher than those at Chalk River. Figure 7 also shows that dry deposition and chemical transformation are the major depletion processes (represented in green color) of NH_3 in the upstream areas while wet

GMDD
5, 2745–2788, 2012

deposition is less important. Southwestern Ontario and northern Ohio were identified as important upstream areas for dry deposition and chemical processes. Dry deposition and chemical transformation of NH_3 occurring en route in those areas reduced NH_3 concentration substantially at both receptor sites. The difference between the two sites in losses due to dry deposition or chemical conversion is smaller than that affected by emissions. The influence of wet deposition is mainly dependent on the precipitation amount and NH_3 concentrations in the upstream areas. Wet deposition occurring in southwestern Ontario, southeastern Pennsylvania, and areas in the vicinity of the two sites affects NH_3 at both sites; however, its influence is the smallest among the four processes mainly because of the sporadic nature of precipitation.

4.3.2 Analysis of contributions of upstream processes

Key atmospheric processes such as diffusion, deposition, and chemical conversion depend on meteorological conditions such as wind direction, wind speed, temperature, and precipitation. Thus, these processes may vary in upstream areas at different times, dynamically affecting the concentrations of a species measured or simulated at a receptor. In order to understand the relative importance of each process, total upstream contributions of each process to the simulated NH_3 and $p\text{-}NH_4^+$ concentrations at the Egbert site were calculated for each simulation hour.

The time series of different upstream process contributions are presented in Fig. 8, along with the simulated NH_3 and $p\text{-}NH_4^+$ concentrations (the net contribution of all those processes) for comparison. Note that negative values here refer to concentration loss whereas positive values denote enhancement. We can see that the simulated concentrations and contributions from each process vary considerably with simulation time, due to changing upstream areas and different behaviours of atmospheric processes in those areas. With the exception of emissions, all other processes reduced NH_3 concentrations. Emission contributions to NH_3 at Egbert vary from 0 to more than $30\,\mu g\,m^{-3}$, with an average of $8\,\mu g\,m^{-3}$. The time series for dry deposition, another surface process, varies in almost the same pattern as from emission contributions.

GMDD
5, 2745–2788, 2012

However, contributions from dry deposition are all negative, with smaller absolute magnitudes. Contributions from dry deposition are within the range from −20 to 0 $\mu g\,m^{-3}$, with an average around −4 $\mu g\,m^{-3}$. The average loss from dry deposition is greater than from chemical conversion that varies between −15 to 0 $\mu g\,m^{-3}$ with an average of −2 $\mu g\,m^{-3}$. Contributions from wet deposition depend on the amount of precipitation and are generally small, with an average less than −1 $\mu g\,m^{-3}$.

Unlike NH_3, the sole contributor to p-NH_4^+ is chemical conversion, with an average around 2 $\mu g\,m^{-3}$, almost equivalent in magnitude to chemical loss of NH_3. Contributions from both dry deposition and wet deposition are approximately within −4 to 0 $\mu g\,m^{-3}$; however, the average of wet deposition is around −0.4 $\mu g\,m^{-3}$, about half of the average of dry deposition contribution.

Figure 9 shows the average contribution from each process over the entire simulation period at all six sites, derived from time-averaging the time series of different process contributions (an example of such time series is Fig. 8 for Egbert). Loss of NH_3 is mainly due to dry deposition and chemical conversion, whereas p-NH_4^+ is depleted primarily by dry deposition and wet deposition. Dry deposition plays an important role for both NH_3 and p-NH_4^+ in reducing their levels in the atmosphere, but wet deposition plays a proportionately larger role for p-NH_4^+ than NH_3. The simulation results indicate that the level of NH_3 could be more than two times higher than the values seen in Fig. 3 if removal processes were absent.

The differences of upstream process contributions to NH_3 are significant between the agricultural sites (Egbert, Longwoods, and St. Mary's) and the forest sites (Chalk River, Sprucedale, and Haliburton). On average, emission contribution, dry deposition, wet deposition, and chemical conversion to the agricultural sites are 2.5, 2.2, 1.6 and 1.7 times the values to forest sites, respectively. For p-NH_4^+, a secondary pollutant with weaker spatial variability and a longer atmospheric lifetime, results indicate much smaller difference between the two groups of sites. Dry deposition, wet deposition and chemical conversion to the agricultural sites are 1.3, 1.1 and 1.7 times the values to forest sites, respectively.

GMDD
5, 2745–2788, 2012

We calculated the ratio of each sink (negative contribution) to total sources (positive contribution) for each site using results displayed in Fig. 9, and the resulting values are shown in Table 4. Ratios of total sinks to total sources are calculated as well. Between the two groups of sites, the difference in ratios of total sinks to total sources is significant. The forest sites are on average 0.20 and 0.22 larger than the agricultural sites for NH_3 and p-NH_4^+, respectively. Out of the 0.20, the difference for NH_3, 65 % is attributed to the difference (0.13) in ratios of chemical conversion to total sources. In the chemical processes of NH_3, the $NH_3/HNO_3/NH_4NO_3$ equilibrium is very sensitive to the temperature (Stelson et al, 1979; Seinfeld and Pandis, 2006). An increase in temperature from 20° C to 30° C could increase the equilibrium gas-phase concentration of NH_3 and HNO_3 (equimolar) from 11.0 to 38.4 μg m^{-3} (Stelson et al, 1979), significantly reducing the gas-to-aerosol chemical conversion of NH_3. We suspect that such a large difference in ratios of chemical conversion to total sources is due to different air temperatures mainly caused by different latitudes of the two groups sites (estimated from NARR dataset of the first layer (975–1000 mb), air temperature mean over the entire simulation period for the forest sites is about 2° C lower than the agriculture sites). For p-NH_4^+, the largest contributor to the difference in ratios of total sinks to total sources between the two groups of sites is dry deposition, accounting for about 64 % (0.14) of total difference (0.22), mainly because the dry deposition velocities of p-NH_4^+ are generally larger for forest surface than crop surface (Zhang et al., 2001).

5 Conclusion and discussion

The STILT-Chem model was improved in this study by incorporating a new chemistry module to simulate atmospheric NH_3 and NH_4^+. Thus, the improved model can be utilized to simulate transport, emission, deposition and chemical transformations for gas-phase species, as well as multi-phase species involved in the key atmospheric reactions of NH_3 and NH_4^+. The model was applied to six measurement sites in Ontario, Canada. Simulated results were evaluated against a unique set of measurements for a

GMDD
5, 2745–2788, 2012

six-month period in 2006. The comparison demonstrated satisfactory performance of the model for p-NH_4^+. Relatively poor performance for NH_3 is likely due to the strong spatial variability of NH_3 and uncertainties in the NH_3 emissions and/or their coarse-scale grid spacing.

The model can also be applied as an effective tool to quantitatively investigate and understand upstream sources, sinks, and atmospheric processes that significantly and frequently affect concentrations at selected receptors since it is a back-trajectory-based model, and the influence of each major process on the simulated or observed concentration at receptors can be calculated for every upstream location at each time step. This kind of application has been demonstrated in the study. The modeled results suggest that the concentrations of NH_3 at those sites were most significantly affected by sources and processes in southwestern Ontario, the northern part of Ohio and nearby areas. NH_3 is mainly contributed by emission sources whereas p-NH_4^+ is mainly from the conversion of NH_3. Dry deposition is the major removal process for both NH_3 and p-NH_4^+ in the atmosphere during the study period.

This study also revealed the contrast between agricultural versus forest sites. Not only were emissions of NH_3 higher in agricultural areas, but removal mechanisms (especially chemical loss for NH_3 and dry deposition for NH_4^+) were more efficient in forests. This combination explains the significantly higher concentrations of NH_3 and NH_4^+ observed at agricultural sites.

Although the improved STILT-Chem can reasonably well simulate atmospheric NH_3 and NH_4^+, the treatment of multi-phase reactions is highly simplified. Only the dominate multi-phase reactions involving ammonia and ammonium were considered in the model. Further development of the model will focus on incorporating major atmospheric aqueous and aerosol chemistry, and a dry deposition scheme that accounts for bi-directional exchange of ammonia into the model.

Acknowledgements. We gratefully acknowledge funding from Environment Canada for supporting D. Wen and for the Canadian Air and Precipitation Monitoring Network data. We thank Q. Zheng and J. Zhang of Environment Canada for preparing the emissions files used in this

GMDD
5, 2745–2788, 2012

study. This work was made possible by the facilities of the Shared Hierarchical Academic Research Computing Network (SHARCNET: www.sharcnet.ca) and Compute/Calcul Canada.

References

Aksoyoglu, S., Keller, J., Barmpadimos, I., Oderbolz, D., Lanz, V. A., Prévôt, A. S. H., and Baltensperger, U.: Aerosol modelling in Europe with a focus on Switzerland during summer and winter episodes, Atmos. Chem. Phys., 11, 7355–7373, doi:10.5194/acp-11-7355-2011, 2011. 2764

Alexander, B., Park, R. J., Jacob, D. J., Li, Q. B., Yantosca, R. M., Savarino, J., Lee, C. C. W., and Thiemens, M. H.: Sulfate formation in sea-salt aerosols: Constraints from oxygen isotopes, J. Geophys. Res., 110, D10307, doi:10.1029/2004JD005659, 2005. 2756

Appel, K. W., Bhave, P. V., Gilliland, A. B., Sarwar, G., and Roselle, S. J.: Evaluation of the Community Multiscale Air Quality (CMAQ) model version 4.5: Sensitivities impacting model performance; Part II–particulate matter, Atmos. Environ., 42, 6057–6066, 2008. 2764, 2765

Asman, W. A. H., Sutton, M. A., and Schjørring, J. A. N. K.: Ammonia: emission, atmospheric transport and deposition, New Phytologist, 139, 27–48, 1998. 2747

Boylan, J. W. and Russell, A. G.: PM and light extinction model performance metrics, goals, and criteria for three-dimensional air quality models, Atmos. Environ., 40, 4946–4959, 2006. 2764

Charlson, R. J. and Rodhe, H.: Factors controlling the acidity of natural rainwater, Nature, 295, 683–685, 1982. 2752

Cheng, Y. H. and Tsai, C. J.: Evaporation loss of ammonium nitrate particles during filter sampling, J. Aerosol Sci., 28, 1553–1567, 1997. 2764

Coats, C.: The EDSS/Models-3 I/O API: User Manual, Baron Advanced Meteorological Systems, available at: http://www.baronams.com/products/ioapi (last access: 30 June 2012), 2003. 2761

Draxler, R. R. and Hess, G. D.: Description of the HYSPLIT 4 modeling system, NOAA Technical Memorandum ERL ARL-224, 1997. 2748, 2749, 2755, 2756, 2758

EMEP: Transboundary photooxidant air pollution in Europe. Calculations of tropospheric ozone and comparison with observations, EMEP/MSC-W Report 2/98, Oslo, Norway, 1998. 2752, 2754

GMDD

5, 2745–2788, 2012

Emmons, L. K., Walters, S., Hess, P. G., Lamarque, J.-F., Pfister, G. G., Fillmore, D., Granier, C., Guenther, A., Kinnison, D., Laepple, T., Orlando, J., Tie, X., Tyndall, G., Wiedinmyer, C., Baughcum, S. L., and Kloster, S.: Description and evaluation of the Model for Ozone and Related chemical Tracers, version 4 (MOZART-4), Geosci. Model Dev., 3, 43–67, doi:10.5194/gmd-3-43-2010, 2010. 2760

Gear, C. W.: Numerical Initial Value Problems in Ordinary Differential Equations, Prentice-Hall, Englewood Cliffs, NJ, 1971. 2751

Gery, M. W., Whitten, G. Z., Killus, J. P., and Dodge, M. C.: A photochemical kinetics mechanism for urban and regional scale computer modeling, J. Geophys. Res., 94, 12925–12956, 1989. 2748, 2751

Granier, C., Guenther, A., Lamarque, J., Mieville, A., Muller, J., Olivier, J., Orlando, J., Peters, J., Petron, G., Tyndall, G., and Wallens, S.: POET, a database of surface emissions of ozone precursors, available at: http://www.aero.jussieu.fr/projet/ACCENT/POET.php (last access: 30 June 2012), 2005. 2760

Hanna, S. R.: Applications in air pollution modeling, in: Atmospheric Turbulence and Air Pollution Modeling, edited by: Nieuwstadt, F. T. M. and van Dop, H., D. Reidel, Norwell, Mass., 358 pp., 1982. 2749

Hicks, B. B.: A climatology of wet deposition scavenging ratios for the United States, Atmos. Environ., 39, 1585–1596, 2005. 2758

Hoffmann, M. R. and Calvert, J. G.: Chemical transformation modules for Eulerian acid deposition models: Vol. II. The aqueous-phase chemistry, Acid Deposition Modeling Project, National Center for Atmospheric Research, 1985. 2752

Lin, J. C., Gerbig, C., Wofsy, S. C., Andrews, A. E., Daube, B. C., Davis, K. J., and Grainger, C. A.: A near-field tool for simulating the upstream influence of atmospheric observations: The Stochastic Time-inverted Lagrangian Transport (STILT) Model, J. Geophys. Res., 108, 4493, doi:10.1029/2002JD003161, 2003. 2748, 2749, 2750

Makar, P. A., Moran, M. D., Zheng, Q., Cousineau, S., Sassi, M., Duhamel, A., Besner, M., Davignon, D., Crevier, L.-P., and Bouchet, V. S.: Modelling the impacts of ammonia emissions reductions on North American air quality, Atmos. Chem. Phys., 9, 7183—7212, doi:10.5194/acp-9-7183-2009, 2009. 2761, 2765

Mesinger, F., DiMego, G., Kalnay, E., Mitchell, K., Shafran, P. C., Ebisuzaki, W., Jovi, D., Woollen, J., Rogers, E., Berbery, E. H., Ek, M. B., Fan, Y., Grumbine, R., Higgins, W., Li,

GMDD
5, 2745–2788, 2012

H., Lin, Y., Manikin, G., Parrish, D., and Shi, W.: North American regional reanalysis, B. Am. Meteorol. Soc., 97, 343–360, 2006. 2759

Morris, J. T.: Effects of nitrogen loading on wetland ecosystems with particular reference to atmospheric deposition, Ann. Rev. Ecol. Syst., 22, 257–279, 1991. 2747

Mozurkewich, M.: The dissociation constant of ammonium nitrate and its dependence on temperature, relative humidity, and particle size, Atmos. Environ., 27, 261–270, 1993. 2753, 2754

Nenes, A., Pandis, S. N., and Pilinis, C.: Continued development and testing of a new thermodynamic aerosol module for urban and regional air quality models, Atmos. Environ., 33, 1553–1560, 1999. 2752

Nopmongcol, U., Koo, B., Tai, E., Jung, J., Piyachaturawat, P., Emery, C., Yarwood, G., Pirovano, G., Mitsakou, C., and Kallos, G.: Modeling Europe with CAMx for the Air Quality Model Evaluation International Initiative (AQMEII), Atmos. Environ., 53, 177–185, 2012. 2756

Ohara, T., Akimoto, H., Kurokawa, J., Horii, N., Yamaji, K., Yan, X., and Hayasaka, T.: An Asian emission inventory of anthropogenic emission sources for the period 1980–2020, Atmos. Chem. Phys., 7, 4419–4444, doi:10.5194/acp-7-4419-2007, 2007. 2760

Pouliot, G., Pierce, T., Denier van der Gon, H., Schaap, M., Moran, M., and Nopmongcol, U.: Comparing emission inventories and model-ready emission datasets between Europe and North America for the AQMEII project, Atmos. Environ., 53, 4–14, doi:10.1016/j.atmosenv.2011.12.041, 2012. 2761

Press, W. H., Teukolsky, S. A., Vetterling, W. T., and Flannery, B. P.: Numerical Recipies: the art of scientific computing, Cambridge University Press, New York, 1992. 2751

Rolph, G. D., Draxler, R. R., and Pena, R. G.: Modeling sulfur concentrations and depositions in the United States during ANATEX, Atmos. Environ., 26, 73–93, 1992. 2752, 2757, 2758

Rolph, G. D., Draxler, R. R., and Pena, R. G.: The use of model-derived and observed precipitation in long-term sulfur concentration and deposition modeling, Atmos. Environ., 27, 2017–2037, 1993. 2752, 2757, 2758

Seinfeld, J. H. and Pandis, S. N.: Atmospheric Chemistry and Physics: From Air Pollution to Climate Change, 2nd Edn., J. Wiley, New York, 2006. 2751, 2769

Sirois, A.: Temporal variation of oxides of sulphur and nitrogen in ambient air in eastern Canada: 1979–1994, Tellus, 49B, 270-291, 1997. 2759

GMDD

5, 2745–2788, 2012

Spellmann, J. W. and Hindmarsh, A. C.: GEARS: Solution of Ordinary Differential Equations Having a Sparse Jacobian Matrix, California University, Livermore Lawrence Livermore Laboratory, 41 pp., 1975. 2751
Stein, A. F., Lamb, D., and Draxler, R. R.: Incorporation of detailed chemistry into a three-dimensional Lagrangian-Eulerian hybrid model: application to regional tropospheric ozone, Atmos. Environ., 34, 4361–4372, 2000. 2751
Stelson, A. W., Friedlander, S. K., and Seinfeld, J. H.: A note on the equilibrium relationship between ammonia and nitric acid and particulate ammonium nitrate, Atmos. Environ., 13, 369–371, 1979. 2769
Tesche, T. W., Morris, R., Tonnesen, G., McNally, D., Boylan, J., and Brewer, P.: CMAQ/CAMx annual 2002 performance evaluation over the eastern US, Atmos. Environ., 40, 4906–4919, 2006. 2764
UNC: SMOKE V2.4 User's Manual, available at http://www.smoke-model.org/version2.4/index.cfm (last access: 8 July 2012), 2009. 2761
US EPA: Guidance on the use of models and other analysis for demonstrating attainment of air quality goals for ozone, $PM_{2.5}$, and Regional Haze, US EPA, Research Triangle Park, NC 2771, 2007. 2764
van Bremen, N., Burrough, P. A., Velthorst, E. J., van Dobben, H. F., de Wit, T., Ridder, T. B., and Reijnders, H. F. R.: Soil acidification from atmospheric ammonium sulphate in forest canopy throughfall, Nature, 299, 548–550, 1982. 2747
van der Werf, G. R., Randerson, J. T., Giglio, L., Collatz, G. J., Kasibhatla, P. S., and Arellano Jr., A. F.: Interannual variability in global biomass burning emissions from 1997 to 2004, Atmos. Chem. Phys., 6, 3423–3441, doi:10.5194/acp-6-3423-2006, 2006. 2760
Vet, R., Li, S.-M., Beaney, G., Belzer, W., Chan, E., Dann, T., Friesen, K., Hayden, K., Hou, A., Iqbal, S., Jones, K., Leithead, A., Liggio, J., Makar, P., Narayan, J., Ro, C.-U., Shaw, M., Sukloff, B., Vingarzan, R., and Qiu, W.: Chapter 6: Characterization of Ambient Ammonia, PM and Regional Deposition across Canada, in: Environment Canada, The 2008 Canadian Atmospheric Assessment of Agricultural Ammonia, Environment Canada, Gatineau, QC, Canada, 2008. 2759
Wen, D., Lin, J. C., Meng, F., Gbor, P. K., He, Z., and Sloan, J. J.: Quantitative assessment of upstream source influences on total gaseous mercury observations in Ontario, Canada, Atmos. Chem. Phys., 11, 1405–1415, doi:10.5194/acp-11-1405-2011, 2011. 2749, 2750

GMDD
5, 2745–2788, 2012

Wen, D., Lin, J. C., Millet, D. B., Stein, A. F., and Draxler, R. R.: A backward-time stochastic Lagrangian air quality model, Atmos. Environ., 54, 373–386, doi:10.1016/j.atmosenv.2012.02.042, 2012. 2748, 2749

Wesely, M. L.: Parameterization of surface resistance to gaseous dry deposition in regional-scale numerical models, Atmos. Environ., 23, 1293–1304, 1989. 2755, 2756

Wexler, A. S. and Clegg, S. L.: Atmospheric aerosol models for systems including the ions H^+, NH_4^+, Na^+, SO_4^{2-}, NO_3^-, Cl^-, Br^-, and H_2O, J. Geophys. Res., 107, 4207, doi:10.1029/2001JD000451, 2002. 2752

Zhang, L., Gong, S., Padro, J., and Barrie, L.: A size-segregated particle dry deposition scheme for an atmospheric aerosol module, Atmos. Environ., 35, 549–560, 2001. 2755, 2756, 2769

Zhang, L., Moran, M., Makar, P., Brook, J., and Gong, S.: Modelling gaseous dry deposition in AURAMS: A Unified Regional Air-quality Modelling System, Atmos. Environ., 36, 537–560, 2002. 2756

Zhang, L., Brook, J. R., and Vet, R.: A revised parameterization for gaseous dry deposition in air-quality models, Atmos. Chem. Phys., 3, 2067–2082, doi:10.5194/acp-3-2067-2003, 2003. 2755

Zhang, L., Vet, R., Wiebe, A., Mihele, C., Sukloff, B., Chan, E., Moran, M. D., and Iqbal, S.: Characterization of the size-segregated water-soluble inorganic ions at eight Canadian rural sites, Atmos. Chem. Phys., 8, 7133–7151, doi:10.5194/acp-8-7133-2008, 2008. 2759

Zhang, X. Q. and McMurry, P. H.: Theoretical analysis of evaporative losses from impactor and filter deposits, Atmos. Environ., 21, 1779–1789, 1987. 2764

GMDD

5, 2745–2788, 2012

Table 1. Information regarding the six measurement sites in this study.

Site	Latitude (°)	Longitude (°)	Species measured	Land Use
Longwoods	42.88470	−81.48056	$p\text{-}NH_4^+$, NH_3	
Egbert	44.23250	−79.78139	$p\text{-}NH_4^+$, NH_3	Agriculture
St. Mary's	43.218	−81.142	NH_3	
Sprucedale	45.42361	−79.48667	$p\text{-}NH_4^+$, NH_3	
Chalk River	46.06278	−77.40472	$p\text{-}NH_4^+$, NH_3	Forest
Haliburton	45.1205	−78.532	NH_3	

GMDD
5, 2745–2788, 2012

Table 2. Definition of statistical metrics.

Parameter	Definition
Unpaired Peak Accuracy (UPA)	$\left(\frac{P_{\text{peak}} - O_{\text{peak}}}{O_{\text{peak}}}\right) \times 100\,\%$
Ratio of the Means (ROM)	$\left(\frac{1}{N}\sum_{i=1}^{N} P_i\right) / \left(\frac{1}{N}\sum_{i=1}^{N} O_i\right)$
Mean Normalized Gross Error (MNGE)	$\frac{1}{N}\sum_{i=1}^{N}\left\lvert\frac{P_i - O_i}{O_i}\right\rvert \times 100\,\%$
Mean Fractional Bias (MFB)	$\frac{1}{N}\sum_{i=1}^{N}\frac{P_i - O_i}{(P_i + O_i)/2} \times 100\,\%$
Mean Fractional Error (MFE)	$\frac{1}{N}\sum_{i=1}^{N}\frac{\lvert P_i - O_i\rvert}{(P_i + O_i)/2} \times 100\,\%$

P_i: prediction at time i; O_i: observation at time i; N: total number of observations; P_{peak}: maximum predicted concentration; O_{peak}: maximum observed concentration.

GMDD
5, 2745–2788, 2012

Table 3. Statistic for predicted NH_3 and $p\text{-}NH_4^+$ concentrations.

Site	UPA(%)		ROM		MFB(%)		MFE(%)	
	NH_3	$p\text{-}NH_4^+$	NH_3	$p\text{-}NH_4^+$	NH_3	$p\text{-}NH_4^+$	NH_3	$p\text{-}NH_4^+$
Longwoods	101.3	−6.5	1.54	1.06	38.8	16.4	41.7	66.9
Egbert	50.3	−22.5	1.43	1.04	36.2	19.9	41.9	69.0
St. Mary's	−26.9		0.80		−20.2		30.6	
Sprucedale	−58.9	−19.2	0.55	1.02	−31.9	22.1	94.7	60.9
Chalk River	6.6	−21.1	1.59	1.08	85.5	32.9	122.3	60.5
Haliburton	27.3		1.51		55.8		69.9	

GMDD
5, 2745–2788, 2012

Table 4. Ratios of each sink term, and total sinks to total sources for NH_3 and NH_4^+.

Type	Site	NH_3				p-NH_4^+		
		TSK/TSC	D/TSC	W/TSC	C/TSC	TSK/TSC	D/TSC	W/TSC
Agriculture	Longwoods	0.69	0.37	0.05	0.27	0.45	0.28	0.17
	Egbert	0.78	0.45	0.06	0.27	0.57	0.37	0.20
	St. Mary's	0.68	0.40	0.05	0.23	0.49	0.32	0.17
Forest	Sprucedale	0.94	0.47	0.08	0.39	0.76	0.47	0.29
	Chalk River	0.90	0.43	0.09	0.39	0.78	0.45	0.33
	Haliburton	0.91	0.47	0.07	0.38	0.72	0.47	0.25

TSK: total sinks. TSC: total sources. D: Dry deposition. W: Wet deposition. C: Chemical conversion. C/TSC = 1.0 for p-NH_4^+ because chemical conversion is the only source.

GMDD
5, 2745–2788, 2012

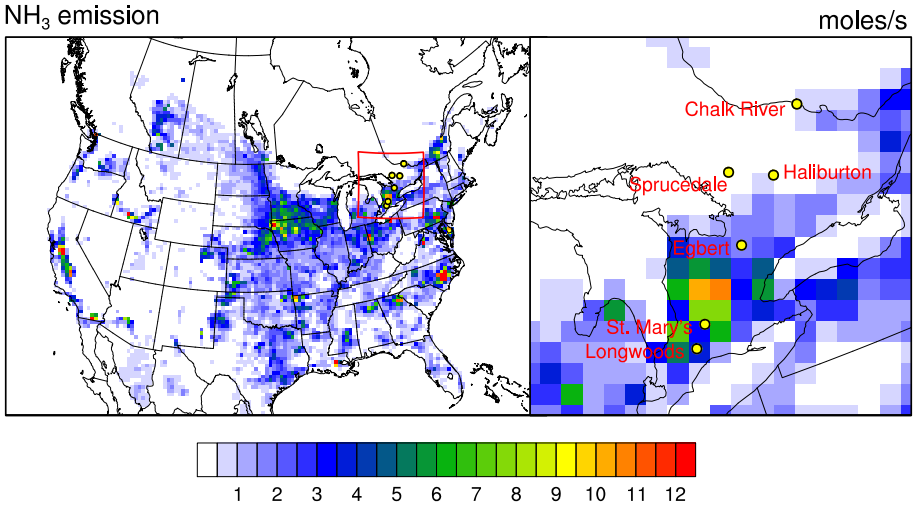

Fig. 1. Spatial distribution of gridded NH_3 emissions over North America (left panel) and locations of six measurement sites and their local NH_3 emission rates averaged over the simulation period (right panel, zooms into the area enclosed by red lines in the left panel).

GMDD
5, 2745–2788, 2012

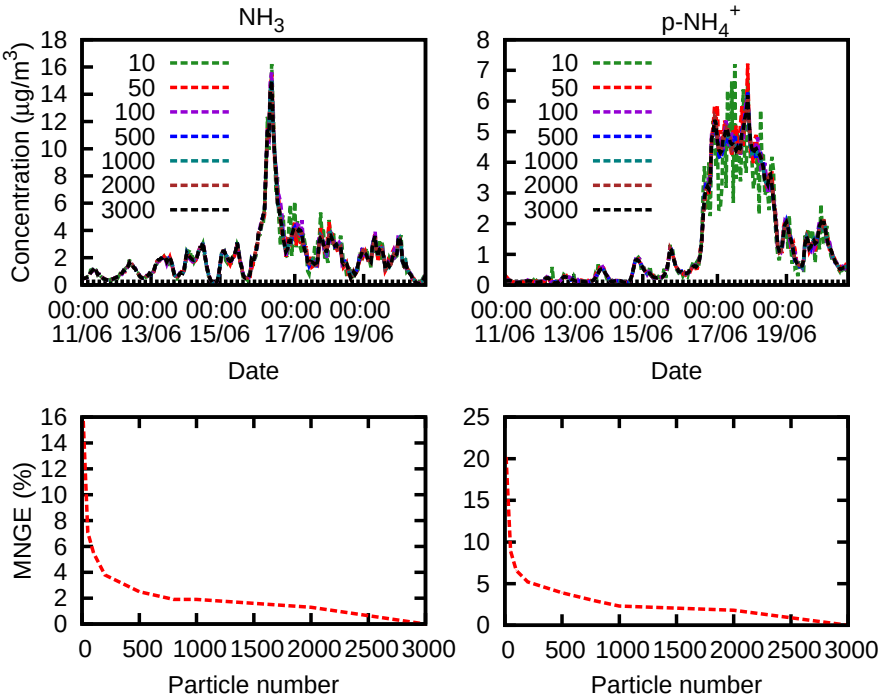

Fig. 2. Sensitivity of the model simulation to the number of particles: modeled NH_3 (left) and $p\text{-}NH_4^+$ (right) concentrations (top) at Egbert with different particle numbers; MNGEs (bottom) of NH_3 (left) and $p\text{-}NH_4^+$ (right) concentration relative to the simulation with 3000 particles.

GMDD
5, 2745–2788, 2012

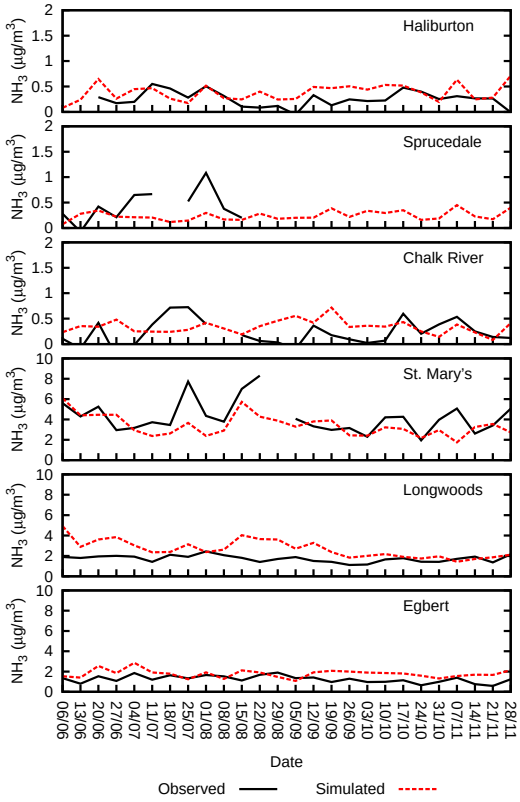

Fig. 3. Modeled (red dash) and measured (black solid) NH_3 concentrations ($\mu g\, m^{-3}$) for each test site during the simulation period from 1 June to 30 November 2006. Note change in scale between upper and lower panels.

GMDD
5, 2745–2788, 2012

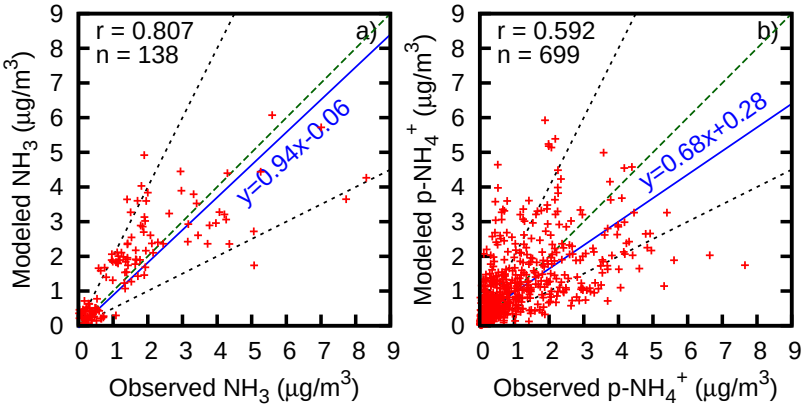

Fig. 4. Correlations between measured and modeled weekly NH_3 concentrations (µg m^{-3}) for six sites (left) and 24-h p-NH_4^+ (right) concentrations (µg m^{-3}) for four sites during the simulation period from 1 June to 30 November 2006. The black dotted lines show agreement within a factor of 2. Fitted regression (blue solid) lines and 1 : 1 (darkgreen dashed) lines are also plotted.

GMDD
5, 2745–2788, 2012

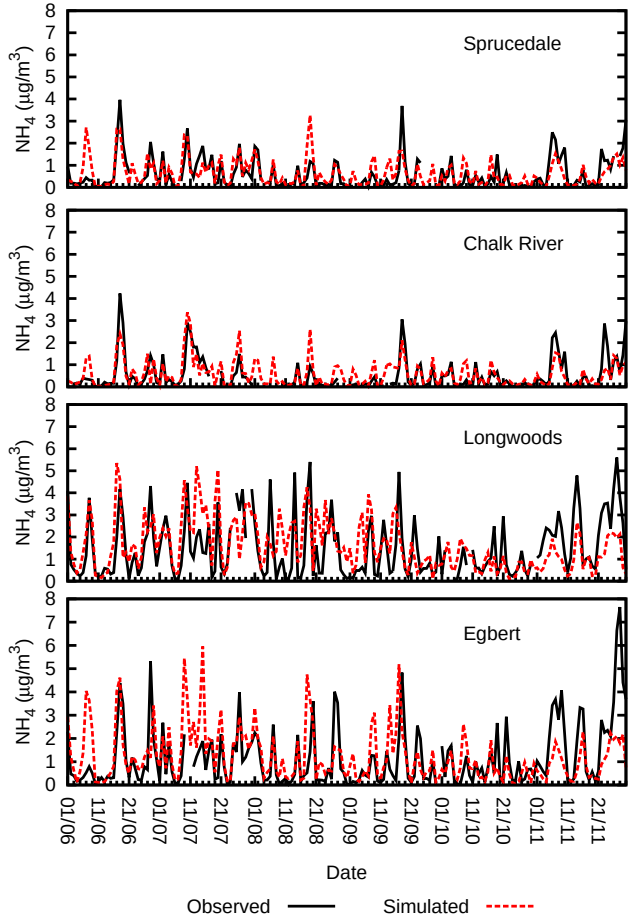

Fig. 5. Modeled (red dash) and measured (black solid) p-NH_4^+ 24-h concentrations (µg m^{-3}) for four test sites during the simulation period from 1 June to 30 November 2006.

GMDD
5, 2745–2788, 2012

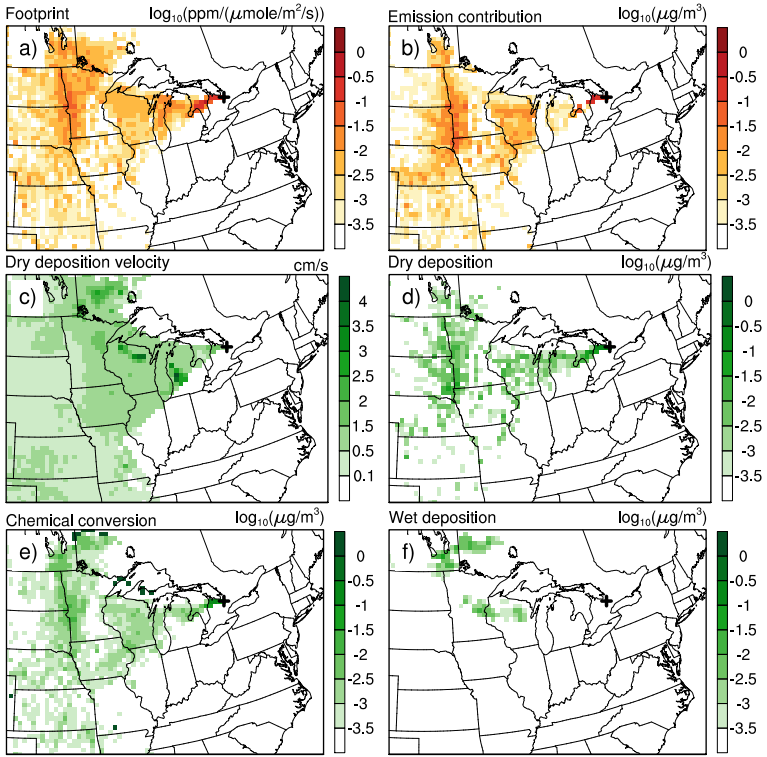

Fig. 6. Modeled upstream parameters and processes impacting NH_3 concentration simulated at Egbert (location indicated by "+") at 18:00 GMT on 2 July 2006, including: **(a)** footprint (i.e., the sensitivity of modeled NH_3 concentration at Egbert at that time to each upstream location); **(b)** emission contribution; **(c)** dry deposition velocity; **(d)** loss due to dry deposition; **(e)** loss due to chemical conversion; and **(f)** loss due to wet deposition.

GMDD
5, 2745–2788, 2012

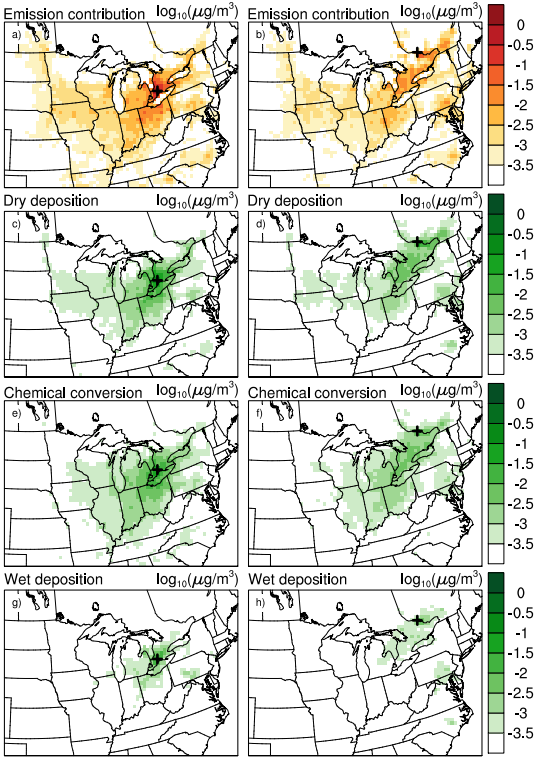

Fig. 7. Modeled upstream contributions to simulated NH_3 concentrations from emission (**a** and **b**); dry deposition (**c** and **d**); chemical conversion (**e** and **f**); and wet deposition (**g** and **h**) over 6 months at two sites: Longwoods (left) and Chalk River (right). Each panel shows an average over the entire simulation period. Red color scale represents positive contributions (source) whereas green scale represents negative contributions (loss). Site locations are indicated by "+".

GMDD
5, 2745–2788, 2012

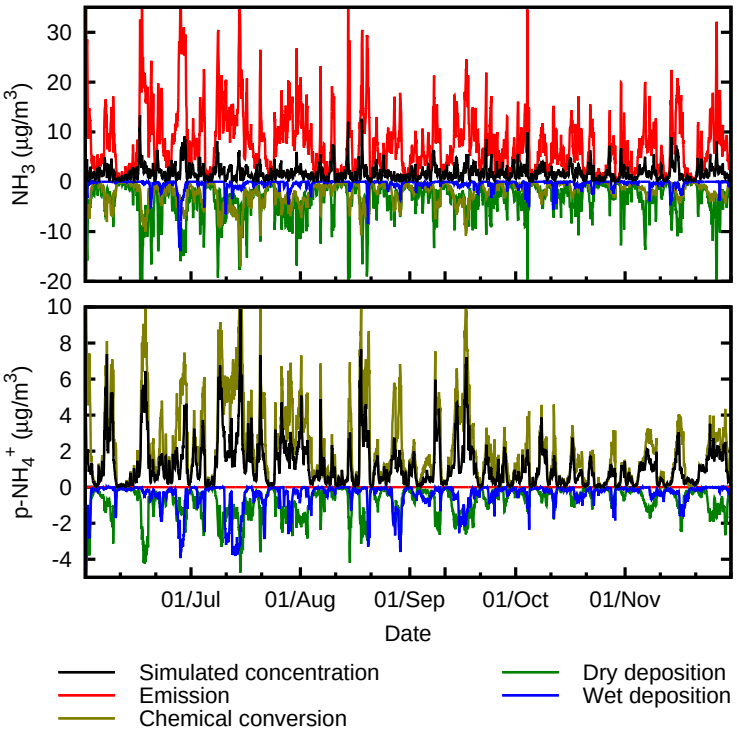

Fig. 8. Simulated NH_3 (top) and p-NH_4^+ (bottom) concentrations (black) at Egbert, compared against modeled contributions from emission (red), dry deposition (green), wet deposition (blue), and chemical conversion (olive) for the entire simulation period.

GMDD
5, 2745–2788, 2012

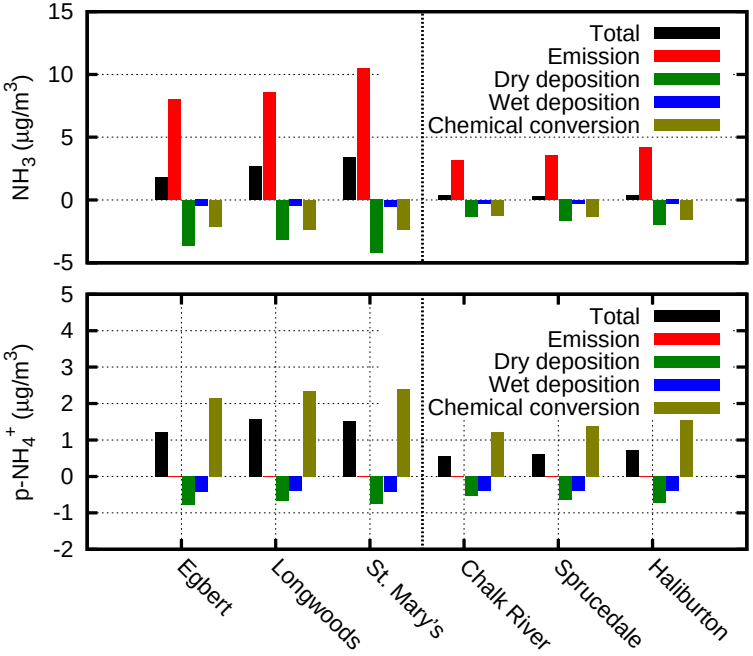

Fig. 9. Mean contributions to NH_3 (top) and p-NH_4^+ (bottom) due to emissions (red), dry deposition (green), wet deposition (blue), and chemical conversion (olive). The total enhancement over the background is shown in black. These mean contributions were obtained by averaging each contribution over the entire six-month simulation period.

GMDD
5, 2745–2788, 2012